

Connecting Star Formation in the Milky Way and Nearby Galaxies -II. An Analytical Model to Predict Cloud-Scale Star Formation Rate

J. W. Zhou ^{★1} Sami Dib ² Pavel Kroupa ^{3,4}

¹Max-Planck-Institut für Radioastronomie, Auf dem Hügel 69, 53121 Bonn, Germany

²Max-Planck-Institut für Astronomie, Königstuhl 17, 69117 Heidelberg, Germany

³Helmholtz-Institut für Strahlen- und Kernphysik (HISKP), Universität Bonn, Nussallee 14–16, 53115 Bonn, Germany

⁴Charles University in Prague, Faculty of Mathematics and Physics, Astronomical Institute, V Holešovičkách 2, CZ-180 00 Praha 8, Czech Republic [†]

Accepted XXX. Received YYY; in original form ZZZ

ABSTRACT

We construct a model by integrating observational results from the Milky Way and nearby galaxies to predict cloud-scale star formation rate (SFR). In the model, we first estimate the initial total mass of clumps in a cloud based on the cloud mass, and then generate the initial clump population of the cloud using the initial clump mass function. Next, we model the star formation history (SFH) of the cloud to assign an age to each clump. We then identify the clumps with ages between 2 and 5 Myr and calculate the total embedded cluster mass. Finally, we predict the SFR based on the duration of the embedded phase. The model-predicted SFR is comparable to the observed SFR, demonstrating the validity of the model.

Key words: – ISM: clouds – galaxies: clusters – galaxies: star formation

1 INTRODUCTION

Galaxies act as stellar factories in the universe, producing stars through the gravitational collapse of the densest regions within molecular clouds. Molecular clouds are widely distributed within galaxies and serve as localized sites for star formation. Each molecular cloud typically contains multiple clumps, which are the local sites of star formation within the cloud and the precursors of embedded star clusters (Kennicutt & Evans 2012; Miville-Deschênes et al. 2017; Rosolowsky et al. 2021; Urquhart et al. 2022; Yan et al. 2017; Zhou et al. 2024d,c). The work of Motte et al. (2018); Vázquez-Semadeni et al. (2019); Kumar et al. (2020); Henshaw et al. (2020); Zhou et al. (2022, 2023, 2024b); Zhou & Davis (2024); Zhou et al. (2024a); Zhou & Li (2025); Zhou et al. (2025b) (and reference therein) present a comprehensive multi-scale investigation of hub-filament structures, examining their morphology, kinematics, and evolution from dense core (~ 1000 AU) to clump (~ 1 pc), molecular cloud (~ 10 – 100 pc), and galaxy-cloud (~ 1000 pc) scales. These observations reveal hierarchical hub-filament structures with self-similar properties spanning sub-parsec to kiloparsec scales, highlighting their crucial role in the star formation process. Within this hierarchy, a dense core serves as a hub within a clump, a clump functions as a hub within a molecular cloud, and a molecular cloud acts as a hub within a galaxy. Hub-filament structures form through the gravitational contraction of gas structures. Velocity gradient analyses suggest that gas inflows along filaments are driven by gravity. Molecular gas is organized into network structures formed by the gravitational coupling of multi-scale hub-filament structures, where local gravitational centers (hubs) serve as the primary sites of star formation.

A thorough understanding of the properties of giant molecular clouds (GMCs) is key to deciphering the connection between gas dynamics and star formation in galaxies. Thanks to high-resolution, multi-wavelength observations, it is now possible to resolve star formation down to the scale of individual molecular clouds in nearby galaxies. In particular, high-resolution CO imaging from ALMA (Atacama Large Millimeter/submillimeter Array), along with other submillimeter observations, enables systematic investigations of the molecular cloud population beyond the Milky Way (Leroy et al. 2021a,b; Lee et al. 2022; Emsellem et al. 2022; Lee et al. 2023; Grishunin et al. 2024; Schinnerer & Leroy 2024). Since molecular clouds in the Milky Way can be resolved down to their internal structures, they provide a crucial reference for understanding the internal composition and star formation processes of molecular clouds in nearby galaxies. Star formation occurs primarily within clumps, the dense substructures of molecular clouds. Star formation observed on molecular cloud scales or larger is essentially an integrated outcome of the activity occurring within these clumps. To truly understand the underlying physics of star formation at those larger scales, it is essential to characterize the star-forming states of individual clumps. This requires turning to the Milky Way as a reference, leveraging surveys such as ATLASGAL and Hi-GAL (Schuller et al. 2009; Urquhart et al. 2022; Molinari et al. 2010; Elia et al. 2021), which are capable of resolving individual clumps, along with numerous ALMA follow-up studies that zoom in on single clumps in detail (Sanhueza et al. 2019; Liu et al. 2020; Motte et al. 2022; Molinari et al. 2025).

In Zhou & Dib (2025), we used CO (2–1) and CO (1–0) data cubes to identify molecular clouds and study their kinematics and dynamics in three nearby galaxies and the inner Milky Way. Molecular clouds in the same mass range across these galaxies show broadly comparable physical properties and similar star formation

[★] E-mail: jwzhou@mpifr-bonn.mpg.de

[†] E-mail: dib@mpia.de

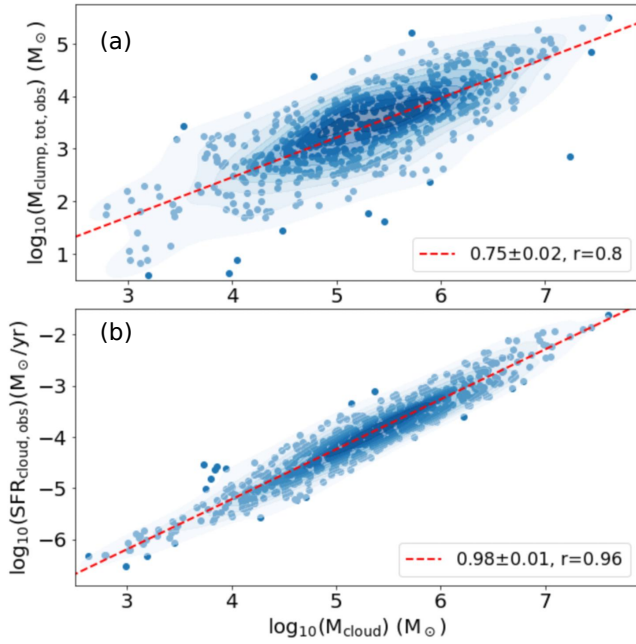


Figure 1. Correlations between the total clump mass in a cloud ($M_{\text{clump,tot,obs}}$), the cloud mass (M_{cloud}) and the SFR of the cloud ($\text{SFR}_{\text{cloud,obs}}$) in the inner Milky Way. r is the correlation coefficient.

rates (SFRs). Strong correlations were found between cloud mass and total clump mass, clump number, and the mass of the most massive clump (see also Zetterlund et al. (2019)). These results suggest that a cloud’s physical conditions regulate its internal clump properties and, in turn, its star-forming potential. Clumps are the true sites of star formation within molecular clouds. In this work, we construct a model to explain cloud-scale observational phenomena (e.g., SFR) using physical scaling laws observed at the clump scale.

2 MODEL

2.1 Correlations from the Milky Way

In Zhou & Dib (2025), we identified molecular clouds in the inner Milky Way using CO (1–0) data cubes and cross-matched them with the ATLASGAL clumps cataloged by Urquhart et al. (2022). Then, we calculated the star formation rate (SFR) surface density of each cloud using the *Spitzer* 24 μm image. Finally, we found strong correlations between the total clump mass in a cloud ($M_{\text{clump,tot,obs}}$), the cloud mass (M_{cloud}) and the SFR of the cloud ($\text{SFR}_{\text{cloud,obs}}$), as shown in Fig. 1. The correlations are

$$\log_{10}(M_{\text{clump,tot,obs}}) = 0.75 \times \log_{10}(M_{\text{cloud}}) - 0.56, \quad (1)$$

$$\log_{10}(\text{SFR}_{\text{cloud,obs}}) = 0.98 \times \log_{10}(M_{\text{cloud}}) - 9.12. \quad (2)$$

In Zhou et al. (2024c), for the ATLASGAL clumps, we found that the clump SFE (star formation efficiency, $\text{SFE}_{\text{clump}}$) decreases with increasing clump mass (M_{clump}), with a median value of ≈ 0.3 . We also derived the correlations between the $\text{SFE}_{\text{clump}}$, the clump mass and the embedded cluster mass (M_{ec1}),

$$\log_{10}(\text{SFE}_{\text{clump}}) = -0.37 \times \log_{10}(M_{\text{clump}}) + 0.42, \quad (3)$$

$$\log_{10}(M_{\text{clump}}) = 1.02 \times \log_{10}(M_{\text{ec1}}) + 0.52. \quad (4)$$

2.2 Clump mass function

Given that clumps represent the progenitors of embedded star clusters, we assume a direct inheritance relationship between the clump mass function (CMF) and the embedded cluster mass function (ECMF). Then we adopt the formalism summarized in (Yan et al. 2017). The CMF is a single slope power law with a variable power-law index, β , that depends on the SFR of the cloud:

$$\xi_{\text{clump}}(M, \text{SFR}) = k_{\text{clump}} \times M^{-\beta(\text{SFR})}, M_{\min} \leq M < M_{\max}, \quad (5)$$

where M_{\min} is the assumed lower limit of clump masses, M_{\max} is the upper integration limit in the optimal sampling method defined in Schulz et al. (2015) and k_{clump} is a normalization constant. The mass of the smallest stellar group observed in Kuhn et al. (2015); Zhou et al. (2024e) is $\approx 5 M_{\odot}$. Thus, we take $M_{\min} = 17 M_{\odot}$, calculated by equation.4.

The parameters k_{clump} and M_{\max} in equation.5 are determined by solving equations.6 & 7 together, i.e., by invoking the clump population mass conservation:

$$M_{\text{clump,tot}} = \int_{M_{\min}}^{M_{\max}} M \xi_{\text{clump}}(M) dM. \quad (6)$$

The optimal sampling normalization condition:

$$1 = \int_{M_{\max}}^{10^9 M_{\odot}} \xi_{\text{clump}}(M) dM, \quad (7)$$

see Yan et al. (2017) for details on the adopted upper integration limit of $10^9 M_{\odot}$. Actually, as long as the upper integration limit is much larger than the real M_{\max} , the result will not be affected. In Sec.2.1, the mass of the most massive clump is only $10^{4.6} M_{\odot}$.

In Elia et al. (2017), for Hi-GAL (Herschel InfraRed Galactic Plane Survey) clumps in the inner Milky Way, the slopes of the CMFs are between -1.88 and -2.46. In Fig.1(b), the SFRs of the clouds in the inner Milky Way are mainly concentrated in the range of 10^{-6} to $10^{-2} M_{\odot}/\text{yr}$. Then we linearly fit the β -SFR relation as

$$\beta = -0.145 \times \log_{10}(\text{SFR}_{\text{cloud,obs}}) + 1.59. \quad (8)$$

2.3 Initial total mass of clumps

Clumps, which are self-gravitating structures within molecular clouds, evolve more rapidly than the clouds themselves. By the time large-scale molecular clouds condense into dense, localized regions within galaxies, star formation has often already taken place within these regions. The molecular clouds we observe are typically composites, containing both exposed and embedded stellar populations, as well as clumps. Nearly all of those stellar populations—whether visible or still embedded—originate from clumps. These clumps may either be currently existing or have existed in the past. Past clumps are now observed as exposed and embedded stellar populations. Together, existing and past clumps constitute the initial clump population of the cloud, described by the initial clump mass function introduced in Sec.2.2. Therefore, $M_{\text{clump,tot}}$ in equation.6 and $M_{\text{clump,tot,obs}}$ in equation.1 are different. $M_{\text{clump,tot}}$ includes both past and present clumps, while $M_{\text{clump,tot,obs}}$ includes only the clumps currently observed. As an estimate,

$$\begin{aligned} M_{\text{clump,tot}} &= M_{\text{clump,tot,obs}} + (M_{\text{emb,tot,obs}} + M_{\text{exp,tot,obs}})/0.3 \\ &= M_{\text{clump,tot,obs}} + M_{\text{cloud}} \times \text{SFE}_{\text{cloud}}/0.3, \end{aligned} \quad (9)$$

where $M_{\text{emb,tot,obs}}$ and $M_{\text{exp,tot,obs}}$ are the total masses of exposed and embedded stellar populations in the cloud, respectively. 0.3 is the median value of the clump-scale SFE (Zhou

et al. 2024c). The SFE of the cloud ($\text{SFE}_{\text{cloud}}$) is defined as, $(M_{\text{emb,tot,obs}} + M_{\text{exp,tot,obs}})/M_{\text{cloud}}$, as calculated in Zhou et al. (2025a),

$$\log_{10}(\text{SFE}_{\text{cloud}}) = -0.32 \times \log_{10}(M_{\text{cloud}}) - 0.034. \quad (10)$$

2.4 Star formation history

Equation.5 defines the initial clump mass function of the cloud. The theoretically initial clump population has now evolved into a mixture of the currently observed clumps and the embedded/exposed stellar populations. The currently observed clumps correspond to the youngest ones, while the embedded and exposed stellar populations can be regarded as the intermediate-age and oldest clumps, respectively. The different components in a molecular cloud — clumps, and embedded and exposed stellar populations — can be regarded as representing the age spread of clumps within the cloud. We then model the star formation history (SFH) of the cloud to distinguish between these different components. Using the SFH models presented in Zhou et al. (2024d); Dib et al. (2025), we examine scenarios where the SFH remains constant and others where it varies over time. Specifically, we create an age distribution of the initial clump population in a cloud to assign an age to each clump. Then, we sort out the intermediate-age clumps, which represent the embedded stellar populations and mainly contribute to the mid-infrared emission of the cloud.

In the cases of a constant SFH, we randomly sample the age of clumps, t_b , with a uniform probability in the age range 0–10 Myr (Yan et al. 2017). For a time-varying SFH, we employ a Gaussian function, allowing us to adjust both the peak position and the distribution width in the 0–10 Myr time range. For this choice of the SFH, the clump age, t_b , is randomly drawn from the Gaussian distribution which is given by:

$$P(t_b) = \frac{1}{\sigma_t \sqrt{2\pi}} \exp\left(-\frac{1}{2} \left(\frac{t_b - t_{b,p}}{\sigma_t}\right)^2\right), \quad (11)$$

where $t_{b,p}$ is the position of the peak and σ_t the standard deviation. In this scenario of burst-like, time-dependent SFH, the t_b values of clumps are randomly chosen based on the probability distribution function $P(t_b)$ as defined in equation.11. We should consider different values of σ_t to cover possible time spans of star formation. We considered values of $t_{b,p} = 2, 4, 6, 8$ Myr and $\sigma_t = 3, 6$ and 9 Myr. There are a total of 12 cases here. Actually, the time-dependent SFH with large σ_t is similar to the flat SFH.

From a clump to an embedded cluster, the formation time is ~ 2 Myr (Evans et al. 2009; Covey et al. 2010; Megeath et al. 2022; Wells et al. 2022; Kim et al. 2023). Thereafter, the duration time of the embedded phase is ~ 2 –5 Myr (Kim et al. 2022, 2023). Therefore, we only select the clumps with ages between 2–5 Myr to calculate the SFR and compare with observations. Equation.4 is used to convert the clump mass to the embedded cluster mass. Then the total embedded cluster mass is divided by the time interval ($t_{\text{emb}} = 3$ Myr) to predict the SFR of the cloud ($\text{SFR}_{\text{cloud,p}}$).

3 RESULTS AND DISCUSSION

3.1 Procedure and prediction

The logic and procedures of the model are as follows: (1) Use equation.9 to estimate the initial total mass of clumps in a cloud; (2) generate the initial clump population in the cloud using the initial

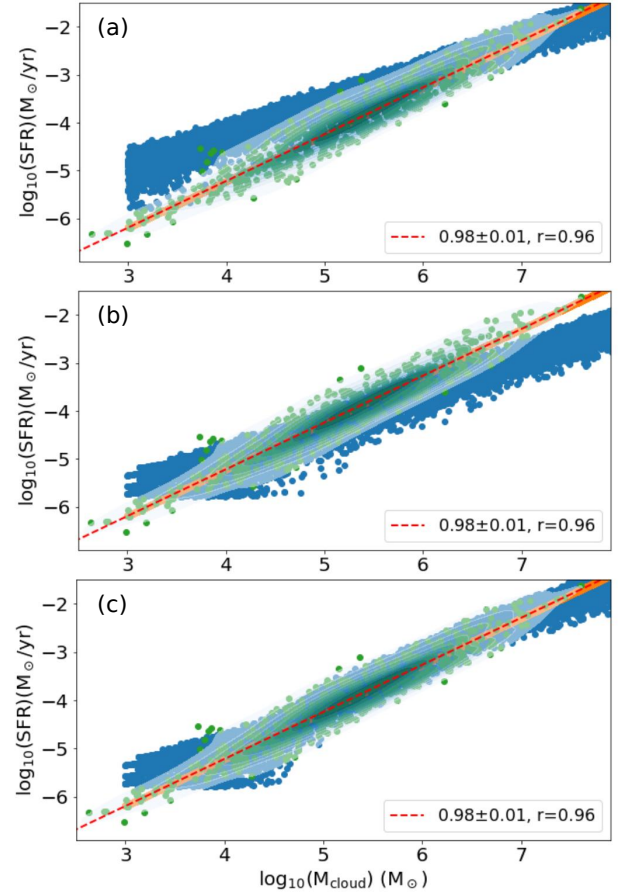


Figure 2. Compare the observed SFR with the model-predicted SFR. (a) Based on equation.9; (b) Based on equation.1; (c) Based on equation.13. r is the correlation coefficient.

clump mass function; (3) model the SFH of the cloud to assign an age to each clump; (4) identify the clumps with ages between 2 and 5 Myr and calculate the total embedded cluster mass; (5) predict the SFR based on the duration of the embedded phase.

In Fig.2(a), for massive clouds, $\text{SFR}_{\text{cloud,p}}$ and $\text{SFR}_{\text{cloud,obs}}$ are comparable, but $\text{SFR}_{\text{cloud,p}}$ is significantly larger than $\text{SFR}_{\text{cloud,obs}}$ for relatively lower mass clouds. If we change equation.9 into equation.1, in Fig.2(b), the result is opposite. Actually, the discussion in Sec.2.3 mainly concerns massive molecular clouds, which can survive for a long time despite hosting stellar populations. In contrast, in low-mass molecular clouds, feedback from the stellar populations can efficiently disrupt the cloud, so they are not expected to contain a significant fraction of stellar components. Equation.10 from Zhou et al. (2025a) is only for clouds with masses larger than $10^{5.5} M_{\odot}$. Therefore, we need a new relation: it should follow equation.9 for high-mass molecular clouds, equation.1 for low-mass molecular clouds, and lie between the predictions of the two equations for intermediate-mass molecular clouds. To obtain a smooth transition between the two regimes, we adopt a linear weighting function defined as

$$t = \frac{x - a}{b - a}, \quad x \equiv \log_{10}(M_{\text{cloud}}/M_{\odot}), \quad (12)$$

where $a = 4.5$ and $b = 7.0$ specify the transition mass range. These two values are determined from Fig.2(a) and (b). t is limited to the range $[0, 1]$. The final relation is then given by

$$M_{\text{clump,tot,m}} = (1 - t) M_{\text{clump,tot,obs}} + t M_{\text{clump,tot}}, \quad (13)$$

where $M_{\text{clump,tot,obs}}$ and $M_{\text{clump,tot}}$ correspond to the relations in equations.1 and equations.9, respectively. After the revision, now the model can well fit the observation, as shown in Fig.2(c).

The total clump mass predicted from the cloud mass significantly affects the results. To accurately estimate the initial total clump mass within a molecular cloud, we need precise measurements of both the current total clump mass and the total stellar mass contained within the cloud. Equation.13 currently represents a compromise, and the exact relationship still needs to be constrained by observations.

3.2 Robustness

We next test the robustness of the model by varying the assumptions set in Sec.2. In Sec.3.1, we modeled a series of star formation histories. However, in Fig.3 and Fig.4, all 13 SFHs produce comparable results, suggesting that the model is insensitive to the SFH of the cloud. For simplicity, a flat SFH was adopted in the following analysis. In Sec.2.1, $\text{SFE}_{\text{clump}}$ varies with clump mass, and consequently, the mass of the embedded cluster formed within the clump also depends on the clump mass. If we assume a constant $\text{SFE}_{\text{clump}}$ ($= 0.3$), in Fig.4(c), the results show no significant change. The slope of the CMF in Sec.2.2 relies on the SFR of the cloud, and the slope ranges from -2.46 to -1.88. In Lada & Lada (2003), the slope of the ECMF is -2. If we take a constant slope -2, in Fig.4(d), the results show no significant change. Therefore, we can conclude that the model is robust.

3.3 Potential caveats

In the model, clumps in molecular clouds are considered to be stable, for example, their masses do not change over time. As discussed in Urquhart et al. (2022), the mass and radius distributions of the ATLASGAL clumps at different evolutionary stages are quite comparable, which implies the stability of the physical properties of the clumps.

We considered three components within the molecular cloud, namely clumps, embedded and exposed stellar populations. The exposed stellar populations have already separated from the gas and therefore do not significantly affect the physical properties of the clumps. As discussed in Zhou et al. (2024f,g), although the embedded stellar populations are spatially closely connected to the clumps, the feedback driven by the embedded stellar populations do not significantly influence the clumps' physical properties. The reason lies in the hierarchical structure of the molecular gas, as described in Sec.1. The network structure of molecular clouds (Zhou et al. 2025b) implies that the knots or local dense structures as local hubs or local gravitational centers are relatively independent of each other. Although some knots in the cloud evolve more rapidly, forming embedded stellar populations, due to their relative independence with the neighboring knots, early feedback from them does not significantly impact the physical properties of the neighboring knots (clumps).

In Urquhart et al. (2022), 5007 ATLASGAL clumps are classified into four evolutionary stages (quiescent, protostellar, young stellar objects and HII regions) and find similar numbers of clumps in each stage. The ATLASGAL clumps with HII regions (HII-clumps) are considered to be in the final stage of star formation and contain fully formed embedded star clusters (Wells et al. 2022; Zhou et al. 2024d,c). Assuming that HII-clumps account for 1/4 of the total number of clumps, and that the typical star formation efficiency of clumps is ~ 0.3 (Zhou et al. 2024c) (and references therein), the fraction of stellar mass contained in the clumps is $\sim 7.5\%$, and can therefore be neglected.

Hence, the potential caveats discussed above can be safely ignored.

4 DATA AVAILABILITY

All data used in this work are available from the first author upon request.

REFERENCES

- Covey, K. R., Lada, C. J., Román-Zúñiga, C., et al. 2010, *ApJ*, 722, 971, doi: [10.1088/0004-637X/722/2/971](https://doi.org/10.1088/0004-637X/722/2/971)
- Dib, S., Zhou, J.-W., Comerón, S., et al. 2025, *A&A*, 693, A51, doi: [10.1051/0004-6361/202450434](https://doi.org/10.1051/0004-6361/202450434)
- Elia, D., Molinari, S., Schisano, E., et al. 2017, *MNRAS*, 471, 100, doi: [10.1093/mnras/stx1357](https://doi.org/10.1093/mnras/stx1357)
- Elia, D., Merello, M., Molinari, S., et al. 2021, *MNRAS*, 504, 2742, doi: [10.1093/mnras/stab1038](https://doi.org/10.1093/mnras/stab1038)
- Emsellem, E., Schinnerer, E., Santoro, F., et al. 2022, *A&A*, 659, A191, doi: [10.1051/0004-6361/202141727](https://doi.org/10.1051/0004-6361/202141727)
- Evans, Neal J., I., Dunham, M. M., Jørgensen, J. K., et al. 2009, *ApJS*, 181, 321, doi: [10.1088/0067-0049/181/2/321](https://doi.org/10.1088/0067-0049/181/2/321)
- Grishunin, K., Weiss, A., Colombo, D., et al. 2024, *A&A*, 682, A137, doi: [10.1051/0004-6361/202347364](https://doi.org/10.1051/0004-6361/202347364)
- Henshaw, J. D., Kruijssen, J. M. D., Longmore, S. N., et al. 2020, *Nature Astronomy*, 4, 1064, doi: [10.1038/s41550-020-1126-z](https://doi.org/10.1038/s41550-020-1126-z)
- Kennicutt, R. C., & Evans, N. J. 2012, *ARA&A*, 50, 531, doi: [10.1146/annurev-astro-081811-125610](https://doi.org/10.1146/annurev-astro-081811-125610)
- Kim, J., Chevance, M., Kruijssen, J. M. D., et al. 2022, *MNRAS*, 516, 3006, doi: [10.1093/mnras/stac2339](https://doi.org/10.1093/mnras/stac2339)
- . 2023, *ApJ*, 944, L20, doi: [10.3847/2041-8213/aca90a](https://doi.org/10.3847/2041-8213/aca90a)
- Kuhn, M. A., Feigelson, E. D., Getman, K. V., et al. 2015, *ApJ*, 812, 131, doi: [10.1088/0004-637X/812/2/131](https://doi.org/10.1088/0004-637X/812/2/131)
- Kumar, M. S. N., Palmeirim, P., Arzoumanian, D., & Inutsuka, S. I. 2020, *A&A*, 642, A87, doi: [10.1051/0004-6361/202038232](https://doi.org/10.1051/0004-6361/202038232)
- Lada, C. J., & Lada, E. A. 2003, *ARA&A*, 41, 57, doi: [10.1146/annurev.astro.41.011802.094844](https://doi.org/10.1146/annurev.astro.41.011802.094844)
- Lee, J. C., Whitmore, B. C., Thilker, D. A., et al. 2022, *ApJS*, 258, 10, doi: [10.3847/1538-4365/ac1fe5](https://doi.org/10.3847/1538-4365/ac1fe5)
- Lee, J. C., Sandstrom, K. M., Leroy, A. K., et al. 2023, *ApJ*, 944, L17, doi: [10.3847/2041-8213/acaaae](https://doi.org/10.3847/2041-8213/acaaae)
- Leroy, A. K., Schinnerer, E., Hughes, A., et al. 2021a, *ApJS*, 257, 43, doi: [10.3847/1538-4365/ac17f3](https://doi.org/10.3847/1538-4365/ac17f3)
- Leroy, A. K., Hughes, A., Liu, D., et al. 2021b, *ApJS*, 255, 19, doi: [10.3847/1538-4365/abec80](https://doi.org/10.3847/1538-4365/abec80)
- Liu, T., Evans, N. J., Kim, K.-T., et al. 2020, *MNRAS*, 496, 2790, doi: [10.1093/mnras/staa1577](https://doi.org/10.1093/mnras/staa1577)
- Megeath, S. T., Gutermuth, R. A., & Kounkel, M. A. 2022, *PASP*, 134, 042001, doi: [10.1088/1538-3873/ac4c9c](https://doi.org/10.1088/1538-3873/ac4c9c)
- Miville-Deschênes, M.-A., Murray, N., & Lee, E. J. 2017, *ApJ*, 834, 57, doi: [10.3847/1538-4357/834/1/57](https://doi.org/10.3847/1538-4357/834/1/57)
- Molinari, S., Swinyard, B., Bally, J., et al. 2010, *A&A*, 518, L100, doi: [10.1051/0004-6361/201014659](https://doi.org/10.1051/0004-6361/201014659)
- Molinari, S., Schilke, P., Battersby, C., et al. 2025, *A&A*, 696, A149, doi: [10.1051/0004-6361/202452702](https://doi.org/10.1051/0004-6361/202452702)
- Motte, F., Bontemps, S., & Louvet, F. 2018, *ARA&A*, 56, 41, doi: [10.1146/annurev-astro-091916-055235](https://doi.org/10.1146/annurev-astro-091916-055235)
- Motte, F., Bontemps, S., Csengeri, T., et al. 2022, *A&A*, 662, A8, doi: [10.1051/0004-6361/202141677](https://doi.org/10.1051/0004-6361/202141677)
- Rosolowsky, E., Hughes, A., Leroy, A. K., et al. 2021, *MNRAS*, 502, 1218, doi: [10.1093/mnras/stab085](https://doi.org/10.1093/mnras/stab085)
- Sanhueza, P., Contreras, Y., Wu, B., et al. 2019, *ApJ*, 886, 102, doi: [10.3847/1538-4357/ab45e9](https://doi.org/10.3847/1538-4357/ab45e9)
- Schinnerer, E., & Leroy, A. K. 2024, *ARA&A*, 62, 369, doi: [10.1146/annurev-astro-071221-052651](https://doi.org/10.1146/annurev-astro-071221-052651)

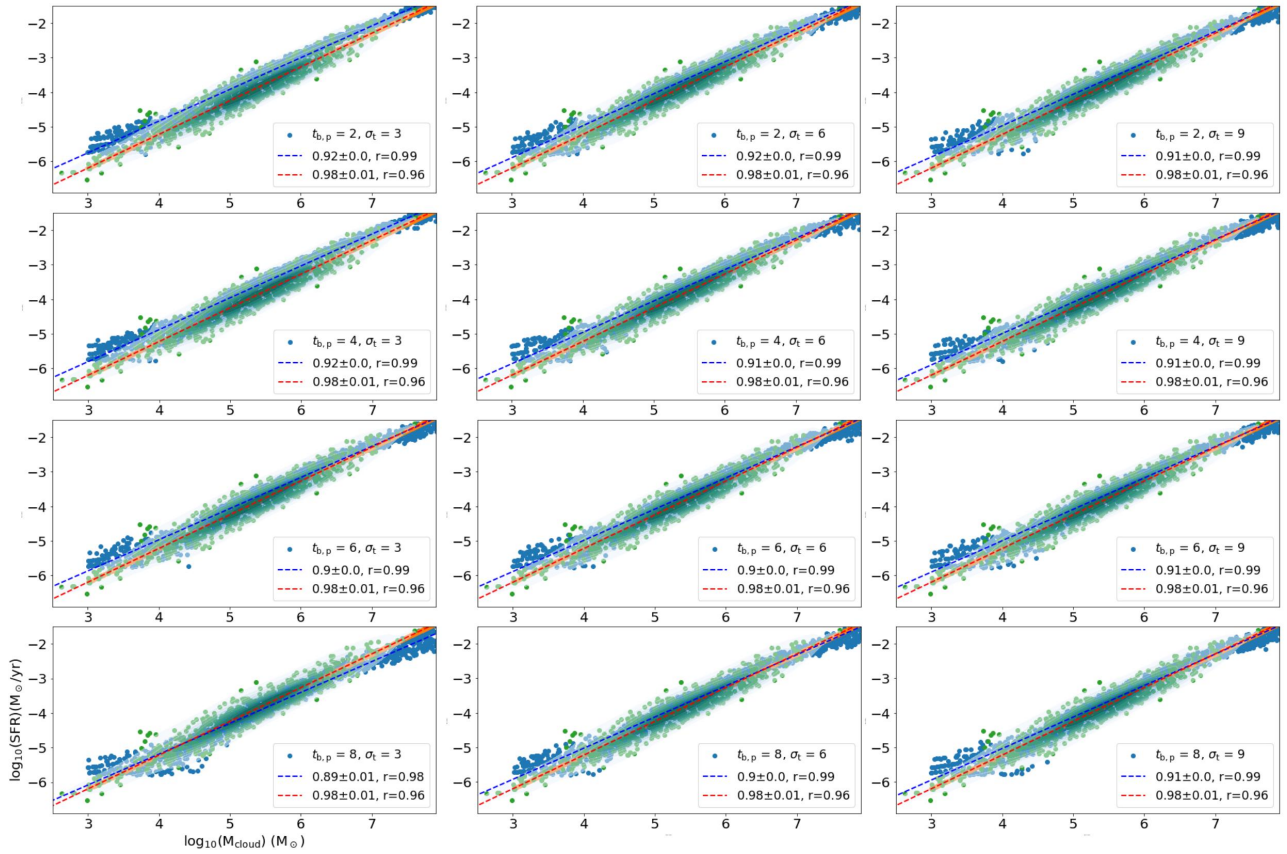


Figure 3. Compare the observed SFR with the model-predicted SFR under 12 Gaussian star formation histories.

Schuller, F., Menten, K. M., Contreras, Y., et al. 2009, *A&A*, 504, 415, doi: [10.1051/0004-6361/200811568](https://doi.org/10.1051/0004-6361/200811568)

Schulz, C., Pflamm-Altenburg, J., & Kroupa, P. 2015, *A&A*, 582, A93, doi: [10.1051/0004-6361/201425296](https://doi.org/10.1051/0004-6361/201425296)

Urquhart, J. S., Wells, M. R. A., Pillai, T., et al. 2022, *MNRAS*, 510, 3389, doi: [10.1093/mnras/stab3511](https://doi.org/10.1093/mnras/stab3511)

Vázquez-Semadeni, E., Palau, A., Ballesteros-Paredes, J., Gómez, G. C., & Zamora-Avilés, M. 2019, *MNRAS*, 490, 3061, doi: [10.1093/mnras/stz2736](https://doi.org/10.1093/mnras/stz2736)

Wells, M. R. A., Urquhart, J. S., Moore, T. J. T., et al. 2022, *MNRAS*, 516, 4245, doi: [10.1093/mnras/stac2420](https://doi.org/10.1093/mnras/stac2420)

Yan, Z., Jerabkova, T., & Kroupa, P. 2017, *A&A*, 607, A126, doi: [10.1051/0004-6361/201730987](https://doi.org/10.1051/0004-6361/201730987)

Zetterlund, E., Glenn, J., & Rosolowsky, E. 2019, *ApJ*, 881, 90, doi: [10.3847/1538-4357/ab2e03](https://doi.org/10.3847/1538-4357/ab2e03)

Zhou, J.-W., & Davis, T. 2024, *Publ. Astron. Soc. Australia*, 41, e076, doi: [10.1017/pasa.2024.47](https://doi.org/10.1017/pasa.2024.47)

Zhou, J. W., & Dib, S. 2025, *arXiv e-prints*, arXiv:2510.26976. <https://arxiv.org/abs/2510.26976>

Zhou, J. W., Dib, S., & Davis, T. A. 2024a, *MNRAS*, 534, 683, doi: [10.1093/mnras/stae2101](https://doi.org/10.1093/mnras/stae2101)

Zhou, J. W., Dib, S., Juvela, M., et al. 2024b, *A&A*, 686, A146, doi: [10.1051/0004-6361/202449514](https://doi.org/10.1051/0004-6361/202449514)

Zhou, J. W., Dib, S., & Kroupa, P. 2024c, *PASP*, 136, 094302, doi: [10.1088/1538-3873/ad77f4](https://doi.org/10.1088/1538-3873/ad77f4)

Zhou, J. W., Kroupa, P., & Dib, S. 2024d, *PASP*, 136, 094301, doi: [10.1088/1538-3873/ad6f44](https://doi.org/10.1088/1538-3873/ad6f44)

Zhou, J.-w., Kroupa, P., & Dib, S. 2024e, *A&A*, 688, L19, doi: [10.1051/0004-6361/202450412](https://doi.org/10.1051/0004-6361/202450412)

Zhou, J. W., Kroupa, P., & Dib, S. 2025a, *MNRAS*, 541, 1276, doi: [10.1093/mnras/staf1070](https://doi.org/10.1093/mnras/staf1070)

Zhou, J. W., & Li, G.-X. 2025, *MNRAS*, 537, 2630, doi: [10.1093/](https://doi.org/10.1093/)

[mnras/staf199](https://arxiv.org/abs/2510.26976)

Zhou, J. W., Urquhart, J. S., Wyrowski, F., et al. 2025b, *A&A*, 699, A355, doi: [10.1051/0004-6361/202554080](https://doi.org/10.1051/0004-6361/202554080)

Zhou, J. W., Wyrowski, F., Neupane, S., et al. 2024f, *A&A*, 682, A128, doi: [10.1051/0004-6361/202347377](https://doi.org/10.1051/0004-6361/202347377)

Zhou, J.-W., Liu, T., Evans, N. J., et al. 2022, *MNRAS*, 514, 6038, doi: [10.1093/mnras/stac1735](https://doi.org/10.1093/mnras/stac1735)

Zhou, J. W., Wyrowski, F., Neupane, S., et al. 2023, *A&A*, 676, A69, doi: [10.1051/0004-6361/202346500](https://doi.org/10.1051/0004-6361/202346500)

Zhou, J. W., Dib, S., Wyrowski, F., et al. 2024g, *A&A*, 682, A173, doi: [10.1051/0004-6361/202348108](https://doi.org/10.1051/0004-6361/202348108)

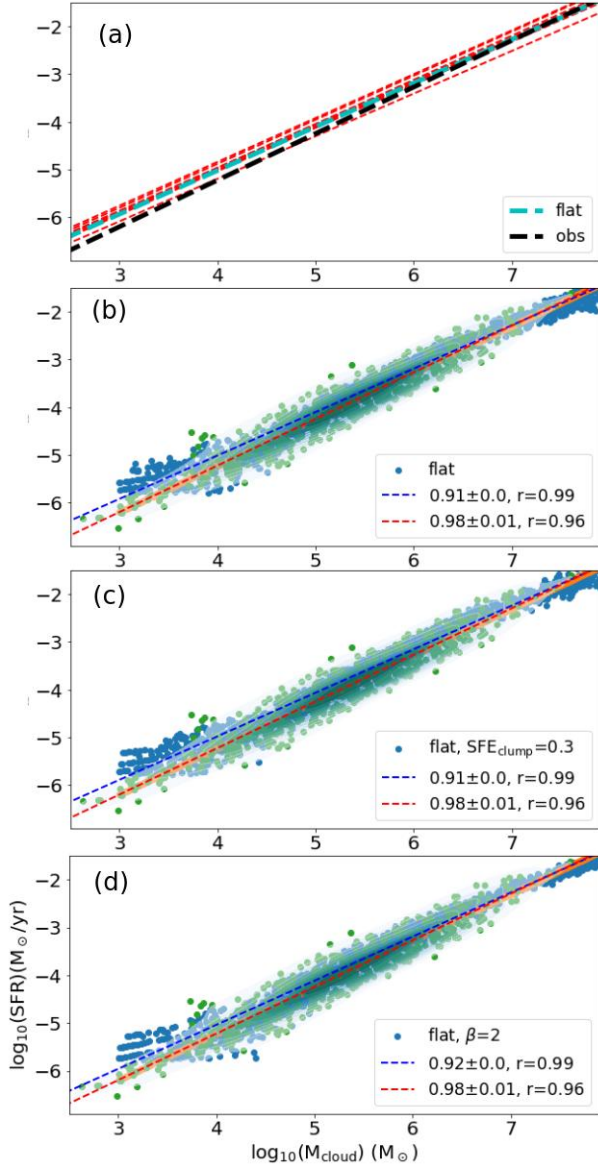


Figure 4. Comparison between the model-predicted SFR and observations under different star formation histories and parameter settings. (a) The black line represents the fit to the observed $\text{SFR}_{\text{cloud,obs}}-M_{\text{cloud}}$ relation; (b) Same as Fig.3, but for the flat star formation history; (c) and (d) Same as panel (b), but $\text{SFE}_{\text{clump}}$ and β are constant.